Shear Banding of Colloidal Glasses: Observation of a Dynamic First-Order Transition

V. Chikkadi, D. M. Miedema, M. T. Dang, B. Nienhuis, and P. Schall
van der Waals–Zeeman Institute, University of Amsterdam, Science Park 904, 1098 XH Amsterdam, Netherlands
(Received 9 January 2014; revised manuscript received 22 June 2014; published 12 November 2014)

We demonstrate that application of an increasing shear field on a glass leads to an intriguing dynamic first-order transition in analogy with equilibrium transitions. By following the particle dynamics as a function of the driving field in a colloidal glass, we identify a critical shear rate upon which the diffusion time scale of the glass exhibits a sudden discontinuity. Using a new dynamic order parameter, we show that this discontinuity is analogous to a first-order transition, in which the applied stress acts as the conjugate field on the system's dynamic evolution. These results offer new perspectives to comprehend the generic shear-banding instability of a wide range of amorphous materials.

DOI: 10.1103/PhysRevLett.113.208301 PACS numbers: 82.70.Dd, 61.43.Fs, 62.20.F-, 64.70.kj

A central unresolved question in the physics of glasses concerns the behavior of a glass under applied stress. While at the glass transition, microscopic observables change rather smoothly, yet rapidly [1,2], as a function of density or temperature; an important question is whether a similarly smooth variation occurs upon application of stress. Recent experiments and simulations show that, unlike quiescent glasses, slowly sheared glasses exhibit high dynamic susceptibilities with long-range, directed strain correlations [3–6]. Such long-range correlations also indicate a high susceptibility to the applied shear. The question is then how the highly susceptible glass responds to an increasing applied shear field.

It is well known that application of shear on amorphous materials can lead to intriguing shear inhomogeneity known as shear banding [7–12], where the shear localizes in bands that flow at a much increased rate. This phenomenon has long been recognized in metallic glasses [8], for which intriguing liquid vein patterns have been observed along the shear bands [12]. Despite its importance to a wide range of amorphous materials including metallic and soft glasses, a fundamental understanding of shear banding is lacking.

Phenomenologically, shear banding is associated with nonmonotonic flow curves [9,13]: the stress to maintain a steady-state flow of the material varies nonmonotonically with applied strain rate. This leads to two (or more) flow rates that coexist at the same applied stress, analogous to the van der Waals description of coexisting gas and liquid. While such nonmonotonic flow curves have been recently measured in colloidal glasses [14], the microscopic origin of shear banding remains unclear; in particular, it is unclear whether and how shear banding is related to structural and dynamic properties of the glassy state. Structural differences in glasses are small, often below the resolution limit, and direct observation of the atomic dynamics in molecular glasses is prohibitively difficult.

Colloidal glasses allow direct observation of single particle dynamics, offering particle trajectories to be followed at long time and large length scales [15,16]. The constituent particles exhibit dynamic arrest due to crowding at volume fractions larger than $\phi_g \sim 0.58$, the colloidal glass transition [17,18]. These systems exhibit glasslike properties such as nonergodicity and aging [19], and they show long-range strain correlations when sheared slowly [5], demonstrating the high susceptibility of the material under applied shear. Recent combined rheology and structure measurements [14] have revealed nonmonotonic flow curves and steady-state shear banding in these systems. The onset of shear banding occurred at shear rates of around the inverse structural relaxation time of the glass, suggesting a deep connection between the shear-banding phenomenon and dynamic properties of the glass. However, the crucial relation between shear banding and glassy dynamics remains unclear: Does the high dynamic susceptibility of the glass eventually lead to a dynamic analog of a first-order transition?

In this Letter, we use direct observation of single particle dynamics in a colloidal glass to show that the application of shear on a glass leads to an intriguing dynamic first-order transition. We demonstrate the existence of a critical shear rate, at which the glass separates into two dynamic states characterized by distinct diffusion time scales. We measure a new dynamic order parameter [20] to demonstrate the coexistence of two dynamic phases. We show that this dynamic transition is accompanied by a weak, but characteristic, structural modification of the glass that relates shear-induced structural distortion to mechanical properties. These results offer a new framework to understand the genuine shear-banding instability observed in a wide range of colloidal and metallic glasses [9,10].

The colloidal glass consists of sterically stabilized fluorescent polymethylmethacrylate particles with a diameter of $\sigma = 1.3$ μm, and a polydisperity of 7%, suspended in a density and refractive index matching mixture of cycloheptyl bromide and *cis*-decalin. A dense suspension with particle volume fraction $\phi \sim 0.60$ well inside the

glassy state is prepared by diluting suspensions centrifuged to a sediment. The suspension is loaded in a cell between two parallel plates 65 μm apart, and a piezoelectric translation stage is used to move the top boundary to apply shear at constant rates between $\dot{\gamma} = 1.5 \times 10^{-5}$ and 2.2×10^{-4} s^{-1}, with a maximum strain of 140%. Confocal microscopy is used to image the individual particles and determine their positions in three dimensions with an accuracy of 0.03 μm in the horizontal and 0.05 μm in the vertical direction [16]. All measurements presented here are recorded in the steady-state regime, after the sample has been sheared to $\gamma \sim 1$. We use the structural relaxation time $\tau = 2 \times 10^4$ s [5] of the quiescent glass to define the dimensionless shear rate $\dot{\gamma}^* = \dot{\gamma}\tau$; the applied shear rates then correspond to $\dot{\gamma}^*$ between 0.3 and 2, smaller and larger than 1, reflecting the transition from the thermal to the shear-dominated regime. We note that this normalized shear rate is significantly lower than in other studies of colloidal flows [11,21].

The shear-rate-dependent flow behavior is summarized in Fig. 1. At shear rates $\dot{\gamma}^* < 1$, the glass flows homogeneously as shown by the particle displacements as a function of height in Fig. 1(a). At $\dot{\gamma}^* > 1$, the glass separates spontaneously into bands that flow at different rates as shown for $\dot{\gamma}^* = 2$ in Fig. 1(b). Linear fits to the displacement profiles yield flow rates of $\dot{\gamma}_{\text{high}} = 2.2 \times 10^{-4}$ s^{-1} and $\dot{\gamma}_{\text{low}} = 4 \times 10^{-5}$ s^{-1} that differ by a factor of 5. We specifically checked for steady state in our measurements, as reaching steady state may require some

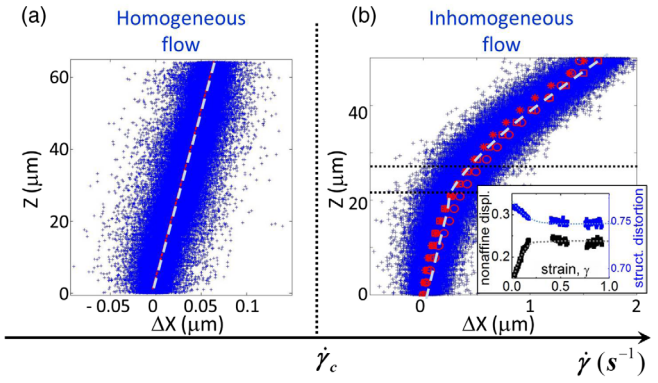

FIG. 1 (color online). Deformation map of colloidal glasses at volume fraction $\phi = 0.60$. The flow is homogeneous at low shear rates (a) and inhomogeneous beyond the critical shear rate $\dot{\gamma}_c \sim 6 \times 10^{-5}$ s^{-1} (b). The figures show height-dependent particle displacements at shear rates $\dot{\gamma} = 3 \times 10^{-5}$ s^{-1} (a) and $\dot{\gamma} = 1 \times 10^{-4}$ s^{-1} (b). Each cross represents a particle. Symbols in (b) indicate average flow profile after $\gamma \sim 0.3$ (circles), 0.8 (squares), and 0.95 (stars), demonstrating stable shear bands. Dashed horizontal lines (b) delineate the shear bands. Inset: Average nonaffine displacement (during $\Delta t = 2$ min, left axis) and structural distortion (eigenvalue ratio of Minkowski tensor W_1^{20} of Voronoi volumes, see Ref. [22], right axis) versus strain demonstrate steady state after $\gamma \sim 0.3$.

larger amount of strain, especially for the shear-banded case. To do so, we first confirm that, after an initial transient, the slopes in Fig. 1(b) remain unchanged over the entire observation time (see red symbols). We then carefully checked both structure and dynamics of the glass as a function of the applied strain. We find that both reach a plateau, conclusively indicating the emergence of steady state for strains larger than $\gamma \gtrsim 0.3$, as shown in Fig. 1(b), inset. We thus observe the spontaneous transition from steady-state homogeneous to steady-state inhomogeneous flow at $\dot{\gamma}^* \sim 1$. This is also in agreement with recent rheology and x-ray scattering measurements [14], revealing shear banding starting at $\dot{\gamma} \sim \tau^{-1}$. This transition from homogeneous to inhomogeneous flow is analogous to the shear banding in metallic glasses [8,12].

To elucidate it, we use the full trajectories of the particles to investigate their dynamic evolution as a function of the applied shear. For each particle i with trajectory $\Delta\mathbf{r_i}(t)$, we subtract the mean flow to compute displacement fluctuations $\Delta\mathbf{r}'_\mathbf{i}(t) = \Delta\mathbf{r_i}(t) - \langle\Delta\mathbf{r}(t)\rangle_z$, where $\langle\Delta\mathbf{r}(t)\rangle_z$ is the average particle displacement at height z. Typical examples of the resulting mean-square displacements $\langle\Delta\mathbf{r}'^2(t)\rangle$ in the high- and low-shear bands are shown in Fig. 2 (inset). The low-shear band (stars) reveals reminiscence of a plateau, while the high-shear band (circles) exhibits a closely linear increase of $\langle\Delta\mathbf{r}'^2(t)\rangle$, similar to the mean-square displacement of particles in a liquid. This interpretation is supported by the strain correlations: strain correlations computed separately for the two bands reveal coexistence of an isotropic liquidlike and an anisotropic solidlike response [5]; similar behavior is observed for all other applied shear rates with $\dot{\gamma}^* > 1$. Interestingly, we can collapse all mean-square displacements by rescaling the time axis by $\dot{\gamma}$ as shown in Fig. 2, main panel. The figure compiles

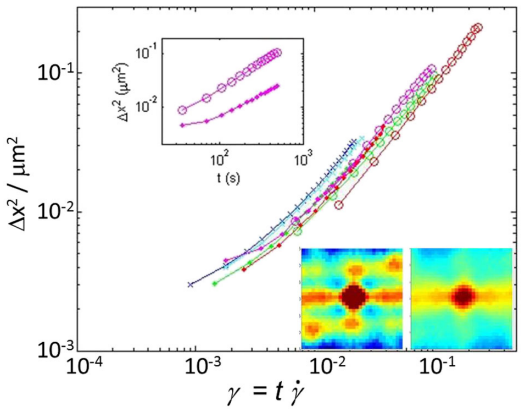

FIG. 2 (color online). Mean-square displacements of the particles. Upper left inset: Mean-square displacement in the upper (circles) and lower shear bands (dots) at $\dot{\gamma}^* = 2$. Main panel: Mean-square displacements as a function of rescaled time for the applied shear rates $\dot{\gamma}^* = 0.3$ (blue), 0.6 (cyan), 1.2 (green), 2 (magenta), and 5.6 (red). Lower right inset: Strain correlations of low shear band for $t = 70$ (left) and 350 s (right).

measurements both in the homogeneous and the shear-banding regime. This collapse suggests that the different dynamics of the bands is solely due to different underlying diffusion time scales. Indeed, this is supported by the strain correlation function that indicates disappearance of the solidlike quadrupolar symmetry when correlations are computed on the rescaled time scale (longer by a factor of $\dot{\gamma}_{\mathrm{high}}/\dot{\gamma}_{\mathrm{low}}$), as illustrated in Fig. 2 (lower right-hand insets). We thus conclude that the change of diffusion time scale causes the symmetry change of correlations; such discontinuous change reminds one of first-order transitions, with the discontinuity occurring in the underlying diffusion time scale.

To quantify this dynamic discontinuity, we search for an order parameter that is a good measure of the dynamic evolution. An appropriate measure of the underlying dynamic evolution is [20]

$$K = \Delta t \sum_{i=1}^{N} \sum_{t=0}^{t_{\mathrm{obs}}} |\Delta \mathbf{r_i}'(t+\Delta t) - \Delta \mathbf{r_i}'(t)|^2, \qquad (1)$$

the time-integrated mean-square displacement, where Δt is a short microscopic time scale. This parameter increases linearly with observation time t_{obs} [Fig. 3(a)]; hence, K/t_{obs} measures the rate of the system's dynamic evolution, and we choose this as the dynamic order parameter. To address the transition, we determine values of K/t_{obs} in 2 μm thick horizontal subsections and plot probability distributions for three different observation times in Fig. 3(b). With increasing observation time, two peaks appear and sharpen, demonstrating the coexistence of two dynamic states. The positions of the peaks demarcate the order parameter values of the coexisting shear bands. We can now construct the corresponding dynamic phase diagram from the peak positions of K for all steady-state shear rates, as shown in Fig. 3(c). At $\dot{\gamma}^* < 1$, only one single peak of K exists, indicating the homogeneous regime. At $\dot{\gamma}^* > 1$, two values coexist, indicating the coexisting shear bands. The diagram has the characteristic topology of a phase diagram, in which the two-phase region is entered close to a critical point. We note that similar dynamic phase coexistence has been recently observed by us in traffic models with interacting cars [23]. With increasing density and in the limit of strong braking, traffic jams exhibited long-range correlations, after which macroscopic phase separation into jammed and free-moving traffic occurred.

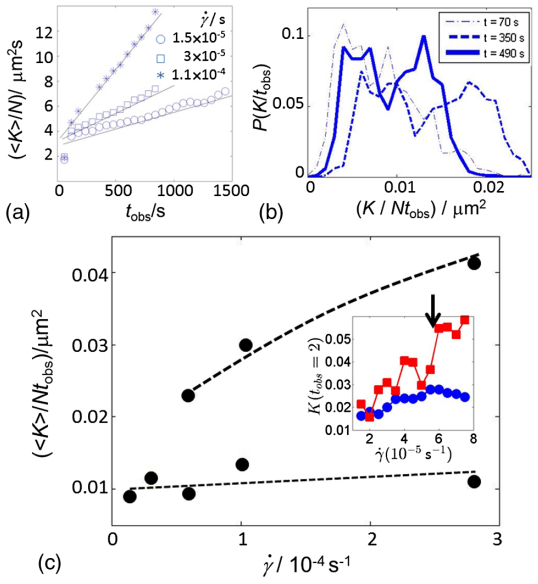

FIG. 3 (color online). Dynamic order parameter and phase diagram. (a) Dynamic order parameter as a function of observation time. K is a linear measure of the system's dynamic evolution. (b) Histogram of order parameter values for increasing observation times. The emerging bimodal distribution indicates dynamic phase coexistence. (c) Corresponding dynamic phase diagram: Mean order parameter as a function of applied strain rate. The dashed lines delineate boundaries of the shear-banding regime. Inset shows the dynamic order parameter at continuously increasing applied shear rate, for particles in the upper (red squares) and lower regions (blue dots). Arrow demarcates sudden change of order parameter.

We confirmed the first-order nature of the transition in x-ray scattering measurements on oscillatory shear [24]. At increasing strain amplitude and concomitant increasing strain rate, the structure factor exhibited an abrupt symmetry change from anisotropic solid to isotropic liquid, just like the strain correlations from confocal microscopy (cf. Fig. 2). These measurements demonstrated the sharpness of the transition: using order parameters to quantify the structural symmetry and its fluctuations, we consistently demonstrated the sharp appearance of a liquidlike state via an abrupt change of the order parameter. The confocal microscope measurements presented here allow us to reveal the microscopic nature of this transition. To elucidate the sharpness as a function of the increasing shear field, we continuously ramped the shear rate $\dot{\gamma}^*$ from below to above 1, crossing the transition with a continuously increasing shear rate. The resulting values of K as a function of strain rate [Fig. 3(c), inset] suggest that, indeed, the transition occurs rapidly, in agreement with our x-ray measurements [24]. Because of the limited system size both spatially and along the time dimension, there are significant fluctuations; nevertheless, the data indicate a sudden jump of the order parameter at $\dot{\gamma}^* \sim 1$. The position of this jump is consistent with the steady-state measurements (main panel), plus an eventual small delay due to metastability [25].

This dynamic transition is surprising and suggests highly collective dynamic behavior of the system. Dynamic first-order transitions have been recently observed in simulations on facilitated glassy dynamics [20]: under an applied artificial field s that couples to the dynamic order parameter distribution via $P(s) = P_0 \exp(-Ks/kT)$, where P_0 is the unperturbed distribution, all hallmarks of a true first-order

transition were observed. In the present case, the applied shear stress σ can take the role of the conjugate field: it is well known that the applied stress σ couples to local rearrangements via their induced strain ϵ according to $P(\epsilon) = P_0 \exp[-\sigma\Omega(\epsilon)/kT]$, where the activation volume $\Omega(\epsilon) = \int \epsilon dV$ measures the integrated local strain [8,26]. Because of the high dynamic susceptibility of the colloidal glass under applied shear [5], likewise, the coupling between the applied stress and the particle dynamics can introduce a first-order transition in its dynamic evolution.

While the transition occurs in the dynamics, it is interesting to elucidate changes in the glass structure. Constitutive models of the flow of amorphous materials suggest a coupling between flow and structure, often related to small density changes [8,11,27]; we therefore investigated structural differences in the two bands. We show radial distribution functions in Fig. 4(a). No obvious structural difference between the low- and high-shear bands is observed, in agreement with earlier observations [11]. However, when we resolve $g(r)$ along the compression and dilation directions, a clear structural difference shows up [Fig. 4(a), inset]. The high-shear band (red symbols and line) exhibits pronounced anisotropy, while the low-shear band (blue symbols and line) is more isotropic. The decrease of $g(r)$ in the dilation direction indicates a depletion of nearest neighbors in the extensional sector, while the (slight) increase of $g(r)$ in the compression direction indicates a (small) enhancement of nearest neighbors in the compressional sector. Because of the nature of the hard-core potential, the increase in the compressional sector is small, smaller than the particle loss in the extensional sector, and this results in a net depletion of particles in the nearest-neighbor cage. According to Ref. [28], this depletion of nearest neighbors leads to lower shear moduli. This is precisely what is observed in the figure: the decrease along the extension direction is more pronounced than the increase in the compression direction, leading to a depletion of particles in the cage. These results reveal the structural origin of the different mechanical behavior of the two bands. This structural distortion should play an important role in the coupling of structure and dynamics in the shear-banding transition. Indeed, we can measure the resulting net dilation in the shear band from the mean-square difference Δ^2 between the two angle-averaged $g(r)$ curves as a function of a linear stretching α that transforms r to $r' = r \times \alpha$. We show Δ^2 as a function of α in Fig. 4(b), inset; the minima of Δ^2 at $\alpha > 1$ indicate a small amount of dilation. We evaluate the minima $\alpha_{\min}$ for all shear rates and plot $\alpha_{\min}$ as a function of shear rate in the main panel. These values indicate a dilation of ~0.4% in the high-shear band after shear banding. While the detected changes are small and affected by large uncertainty, they demonstrate a characteristic structural change accompanying the shear-banding transition.

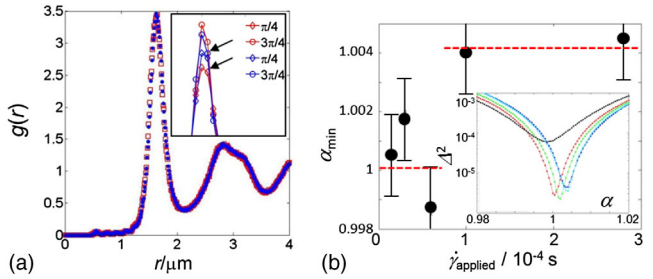

FIG. 4 (color online). Glass structure and density. (a) Pair correlation function of particles in the low- (blue dots) and high-shear bands (red squares). Inset: Angle-resolved $g(r)$ along the shear-shear gradient plane, extension ($\pi/4$, diamonds) and compression direction ($3\pi/4$, circles), for the low- (blue) and high-shear bands (red). Arrows indicate decrease of $g(r)$ in the extension direction. (b) Dilation parameter $\alpha_{\min}$ versus shear rate determined from the minimum of the mean-square difference of $g(r)$ (inset). Dashed lines are guides to the eye.

The direct observation of particle dynamics during shear banding of a colloidal glass reveals the coexistence of two dynamic steady states analogous to the coexistence of equilibrium phases in first-order transitions. The applied shear plays the role of a conjugate field that couples to the dynamic evolution: sufficiently high values of the applied shear rate cause coexistence of two dynamic states with different time scales for diffusion. This mechanism points out new perspectives to comprehend flow instabilities in amorphous materials: the large dynamic susceptibility, on the one hand (evidenced by long-range strain correlations), and the coupling to the applied shear, on the other hand, lead to a dynamic transition that is akin to first-order transitions. This is supported by the different structure of the two bands, distinct by the degree of distortion of the nearest-neighbor cage. This distortion leads to net depletion of particles in the cage, and to lower shear moduli. We believe that the presented dynamic transition should be a general feature of dynamically driven systems, and recent traffic simulations reveal the formation of dynamic condensates in one-dimensional dynamically facilitated systems, consistent with this idea [23]. The observed coupling between applied stress and diffusion time could play a role in crowded biological systems; as the diffusion time scale is an important underlying time scale, any direct coupling of diffusion to external (shear) fields would greatly affect the diffusive behavior upon mechanical perturbation.

This work was supported by the Foundation for Fundamental Research on Matter (FOM), which is subsidized by the Netherlands Organisation for Scientific Research (NWO). We thank D. Denisov for discussion. P. S. acknowledges Vidi and Vici fellowships from NWO.

[1] M. D. Ediger, C. A. Angel, and S. R. Nagel, J. Phys. Chem. **100**, 13200 (1996).

[2] P. N. Pusey and W. van Megen, Phys. Rev. Lett. **59**, 2083 (1987).
[3] C. E. Maloney and M. O. Robbins, Phys. Rev. Lett. **102**, 225502 (2009).
[4] A. Lemaitre and C. Caroli, Phys. Rev. Lett. **103**, 065501 (2009).
[5] V. Chikkadi, G. Wegdam, D. Bonn, B. Nienhuis, and P. Schall, Phys. Rev. Lett. **107**, 198303 (2011).
[6] V. Chikkadi, S. Mandal, B. Nienhuis, D. Raabe, F. Varnik, and P. Schall, Europhys. Lett. **100**, 56001 (2012).
[7] J. S. Langer, Phys. Rev. E **70**, 041502 (2004); Y. Shi, M. B. Katz, H. Li, and M. L. Falk, Phys. Rev. Lett. **98**, 185505 (2007).
[8] F. Spaepen, Acta Metall. **25**, 407 (1977).
[9] P. Schall and M. van Hecke, Annu. Rev. Fluid Mech. **42**, 67 (2010).
[10] A. L. Greer, Y. Q. Cheng, and E. Mad, Mater. Sci. Eng. **R74**, 71 (2013).
[11] R. Besseling, L. Isa, P. Ballesta, G. Petekidis, M. E. Cates, and W. C. K. Poon, Phys. Rev. Lett. **105**, 268301 (2010).
[12] F. Spaepen, Acta Metall. **23**, 615 (1975).
[13] S. Fielding, Soft Matter **3**, 1262 (2007).
[14] D. Denisov, T. Dang, B. Struth, G. H. Wegdam, and P. Schall, Sci. Rep. **3**, 1631 (2013).
[15] P. Schall, D. A. Weitz, and F. Spaepen, Science **318**, 1895 (2007).
[16] E. R. Weeks, J. C. Crocker, A. C. Levitt, A. B. Schofield, and D. A. Weitz, Science **287**, 627 (2000).
[17] W. van Megen, T. C. Mortensen, S. R. Williams, and J. Müller, Phys. Rev. E **58**, 6073 (1998).
[18] P. N. Pusey and W. van Megen, Nature (London) **320**, 340 (1986).
[19] J. P. Bouchaud, J. Phys. I (France) **2**, 1705 (1992).
[20] L. O. Hedges, R. L. Jack, J. P. Garrahan, and D. Chandler, Science **323**, 1309 (2009); D. Chandler and J. P. Garrahan, Annu. Rev. Phys. Chem. **61**, 191 (2010).
[21] C. Eisenmann, C. Kim, J. Mattsson, and D. A. Weitz, Phys. Rev. Lett. **104**, 035502 (2010).
[22] G. E. Schröder-Turk, W. Mickel, M. Schröter, G. W. Delaney, M. Saadatfar, T. J. Senden, K. Mecke, and T. Aste, Europhys. Lett. **90**, 34001 (2010).
[23] A. S. de Wijn, D. M. Miedema, B. Nienhuis, and P. Schall, Phys. Rev. Lett. **109**, 228001 (2012).
[24] D. Denisov, T. Dang, B. Struth, G. H. Wegdam, and P. Schall, arXiv:1401.2106.
[25] We note that first-order transitions are typically associated with metastability leading to time delay when such transitions are crossed dynamically. In our case here, this effect should be small due to the (almost) identical structure of the coexisting dynamic states; see Fig. 4. While a possible small delay of the transition due to metastability is consistent with our data, we cannot conclude on its magnitude.
[26] H. Eyring, J. Chem. Phys. **4**, 283 (1936).
[27] J. S. Langer, Phys. Rev. E **77**, 021502 (2008); E. Bouchbinder and J. S. Langer, Phys. Rev. E **80**, 031133 (2009); Phys. Rev. Lett. **106**, 148301 (2011).
[28] A. Zaccone and E. M. Terentjev, Phys. Rev. Lett. **110**, 178002 (2013); A. Zaccone and E. Scossa-Romano, Phys. Rev. B **83**, 184205 (2011).